Thermoelectric properties of *p*-type LiZnSb: Assessment of *ab initio* calculations

Eric S. Toberer,[a] Andrew F. May, Cidney J. Scanlon, and G. Jeffery Snyder
Materials Science, California Institute of Technology, Pasadena, California 91125, USA

(Received 25 November 2008; accepted 27 January 2009; published online 17 March 2009)

In response to theoretical calculations on the thermoelectric performance of LiZnSb, we report the pertinent transport properties between room temperature and 523 K. Nominal LiZnSb samples are found to be *p*-type, with a carrier concentration in the range $(4-7)\times 10^{20}$ cm^{-3}. The thermoelectric figure of merit (zT) is found to be 0.02–0.08 at 523 K. Analysis of material transport parameters and previously reported *ab initio* calculations demonstrates that even with optimal doping, *p*-type LiZnSb is unlikely to achieve $zT>0.2$ at 523 K. The accuracy of the high zT estimate ($zT>2$) for *n*-type compositions from *ab initio* calculations is discussed within the current synthetic limits.
 [DOI: 10.1063/1.3091267]

I. INTRODUCTION

The development of a high efficiency thermoelectric material remains an outstanding challenge.[1] Such an unprecedented material would lead to the widespread use of thermoelectric materials for efficient, solid state refrigeration, and electricity production. The scalability and simplicity of thermoelectric generators makes them particularly attractive for electricity generation from waste heat and cogeneration sources. As a heat engine, the conversion efficiency of a thermoelectric generator is determined by the product of the Carnot efficiency and a material-dependent term which is an increasing function of the material figure of merit (zT). The thermoelectric figure of merit is determined by the Seebeck coefficient (α) and the electrical (σ) and thermal (κ) conductivity,

$$zT = \frac{\alpha^2\sigma}{\kappa}T.$$

One of the great opportunities for research in thermoelectric materials is the use of robust computational methods to predict transport properties. Computational studies complement experimental work in several ways: (a) a large number of compounds can be screened for thermoelectric performance, (b) predictions of optimum carrier concentrations can guide doping studies, and (c) aid in the explanation of transport properties in current state-of-the-art thermoelectric materials to facilitate the discovery of similar compounds.[2] Much of the prior work involving band structures of thermoelectrics has focused on explaining experimentally observed transport behavior and predicting chemical modifications for improved performance.[3] Purely computational approaches to predict thermoelectric transport behavior are nontrivial because computational zT values require (at a minimum) values for the carrier relaxation time, τ, and lattice thermal conductivity, κ_L. In 2006, Madsen[4] developed an algorithm to screen antimony containing compounds (~500 examined) for thermoelectric performance using band structure calculations and semiclassical Boltzmann theory. Constant values of $\tau = 2\times 10^{-14}$ s and $\kappa_L = 2$ W/m/K were utilized by Madsen.

The most promising material in Madsen's investigation was LiZnSb, with an estimated $zT\sim 2$ at 600 K (for transport in the *ab* plane) when doped *n*-type to $\sim 8\times 10^{19}$ cm^{-3} ($0.01e^-$/u.c.). High thermoelectric efficiency in a compound containing Zn and Sb is not unprecedented; alloys of Zn–Sb were investigated for thermoelectric effects as early as 1823.[5] The stoichiometric compound ZnSb has a peak zT of 0.6 at ~600 K and more recently Zn_4Sb_3 has shown a peak zT of 1.3 at 943 K.[6] Ternary compounds based on Zn and Sb have also shown promise for thermoelectrics: $Ca_{1-x}Yb_xZn_2Sb_2$ exhibits a peak zT of ~0.6 and the structurally distinct $BaZn_2Sb_2$ has a peak zT of 0.3.[7,8] The good thermoelectric properties of Zn–Sb based materials are largely attributed to the similar electronegativity of Zn and Sb and high Sb atomic number, which lead to good carrier mobility and low lattice thermal conductivity, respectively. In the case of Zn_4Sb_3, atomic disorder further reduces the lattice thermal conductivity.[9]

Here, we describe the thermoelectric properties of *p*-type LiZnSb between room temperature and 523 K. Analysis of the Seebeck coefficient, Hall effect, and electrical and thermal conductivities allows the examination of the assumptions utilized in Madsen's automated search for thermoelectrics. The *p*-type conduction reported here limits the ability of the authors to discuss the potential performance of *n*-type LiZnSb.

II. EXPERIMENTAL

The LiZnSb samples were prepared by direct reactions of Li (99.9%), Zn (99.99%), and Sb (99.99%) in boron nitride crucibles encased in evacuated fused silica ampoules. The samples were heated at 923 K for 4 h, and then ball milled with stainless steel vials and balls in a SPEX CertiPrep 8000 Series MixerMill. Dense ingots were formed by hot pressing at 680 K, with ~1.4 metric tons over a 12 mm diameter graphite die. Samples were then sliced into 1 mm thick disks.

[a]Author to whom correspondence should be addressed. Electronic mail: etoberer@caltech.edu.

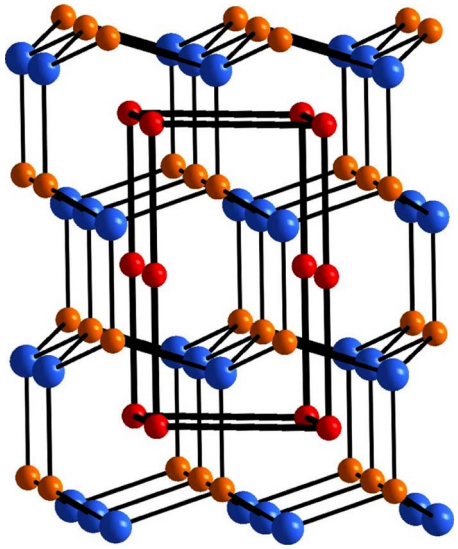

FIG. 1. (Color online) LiZnSb is built of a wurtzite structure of Zn–Sb with interstitial lithium ions (red).

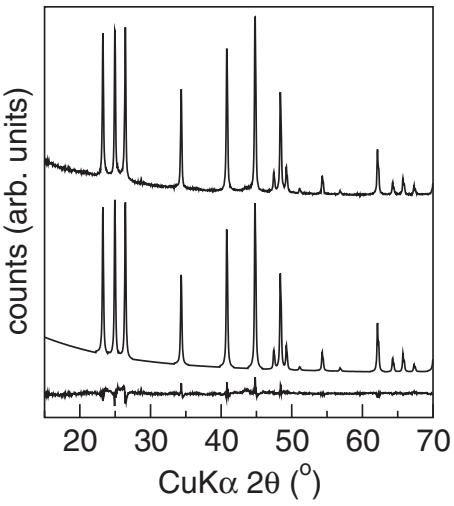

FIG. 2. Powder XRD pattern, Rietveld refinement to the $P6_3mc$ LiZnSb structure, and difference profile.

Structure and phase purity were examined using the X'Pert Plus Rietveld refinement software on x-ray diffraction (XRD) patterns obtained with a Philips X'Pert diffractometer. Transport properties were obtained under dynamic vacuum to 523 K. This maximum temperature was chosen to avoid unintentional changes in chemical composition (and thus transport properties) which may result from sublimation or oxidation. The electrical resistivity was measured using the van der Pauw method and the Hall coefficient was measured with a 2 T field. The Seebeck coefficient was measured using a 10 K temperature gradient as described previously.[10] A Netzsch LFA 457 flash diffusivity instrument was used to measure the thermal diffusivity. To calculate the thermal conductivity, the specific heat of LiZnSb was approximated using the method of Dulong–Petit ($C_{\mathrm{DP}}=3k_B$ per atom, where k_B is Boltzmann's constant). Following characterization to 523 K, resistivity and Seebeck coefficient measurements were conducted under dynamic vacuum to 800 and 750 K, respectively, to observe phase stability.

III. RESULTS AND DISCUSSION

A. Phase purity

Dense, homogeneous ingots of LiZnSb were formed by the sequence of melting, ball milling, and hot pressing. The samples were found to be air sensitive; sample surfaces were polished prior to measurement. The structure of LiZnSb, shown in Fig. 1, is composed of a wurtzite structure of Zn and Sb with Li atoms in trigonal prismatic interstitial sites in the wurtzite structure (3 Zn above, 3 Sb below). Analysis of the XRD pattern using the Rietveld method with the $P6_3mc$ LiZnSb structure revealed a single phase material with lattice parameters $a=4.4281$ and $c=7.1535$ Å (Fig. 2).[11]

B. Transport property measurements and analysis

The electrical resistivity, Seebeck coefficient, and thermal diffusivity were characterized to assess the thermoelectric performance of LiZnSb. To aid in the analysis of these results, Hall effect measurements were also performed.

The samples were found to be p-type, with room temperature Hall carrier concentrations ($p_H=1/R_He$) between approximately 4 and 7×10^{20} cm^{-3} for unintentionally doped (UID) compositions. Figure 3(a) shows the carrier concentrations rise only slightly with increasing temperature, indicating the dominance of extrinsic carriers. From the resistivity (ρ) and Hall carrier concentration, the Hall mobility [μ_H, Fig. 3(b)] may be extracted ($\sigma=1/\rho=p_He\mu_H$). The Hall mobility decreases with increasing temperature and is well characterized by $T^{-1.5}$ decay when a residual mobility is included, which is expected for a heavily doped semiconductor with carrier mobility limited by acoustic phonon scattering. The near constant carrier concentration and temperature dependent mobility leads to an increase in the electrical resistivity with increasing temperature [Fig. 3(c)]. The minor increase in carrier concentration with increasing temperature may be due to minority carriers. Unfortunately, the Hall effect data cannot be analyzed by a multicarrier model without knowledge regarding the mobility of both carrier types. When electrons and holes are present during a Hall effect measurement, the single band Hall carrier concentration will be overestimated because electrons and holes negate the voltage produced by one another.

The Seebeck coefficient (Fig. 4) is positive and rises with temperature up to 523 K, confirming that this is a heavily doped p-type semiconductor. A comparison of our experimental Seebeck coefficient and Madsen's *ab initio* results at 500 K (Fig. 5) shows remarkable agreement between theory and experiment. Analysis of the Seebeck coefficient and carrier concentration allow a parabolic band effective mass (m^*) of ~0.7 m_e to be estimated via classic solutions to the Boltzmann transport equation within the constant relaxation time approximation (CRTA) (this assumes scattering is independent of energy; if acoustic scattering is assumed $m^*/m_e\sim1$ is obtained).[12] Such a calculation allows the *ab initio* results (dashed line in Fig. 5) to be compared to a single parabolic band (SPB) model (solid line in Fig. 5). Figure 5 demonstrates that a SPB model describes the *ab*

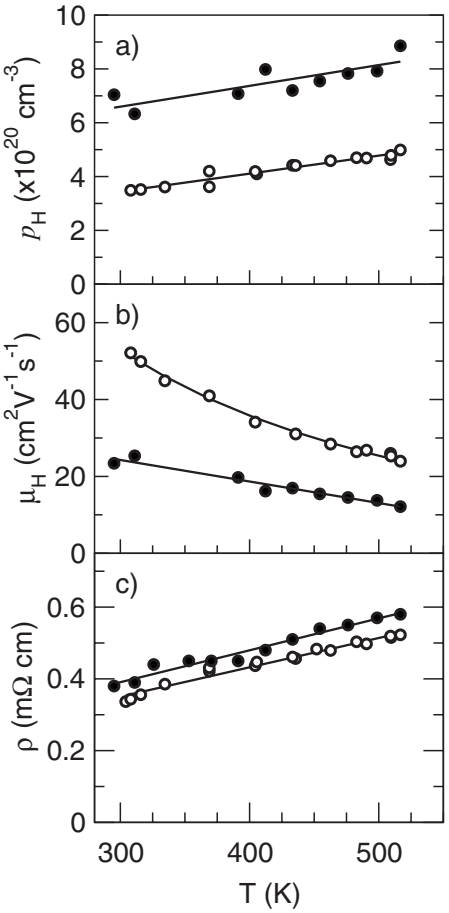

FIG. 3. Hall effect and van der Pauw resistivity results from two on-stoichiometry samples of LiZnSb. (a) The carrier concentration is dominated by extrinsic holes and (b) the mobility decays with temperature, leading to a (c) resistivity that rises linearly, as one would expect for a heavily doped semiconductor.

initio results well at high carrier concentrations, but deviates at low carrier concentrations. The deviation at low carrier concentrations is due to the multiband features present in the *ab initi*o calculation. To account for such features in the single band model, the effective mass would need to be a function of carrier concentration.

Higher temperature measurements of the resistivity under dynamic vacuum reveal rapid sublimation beginning at

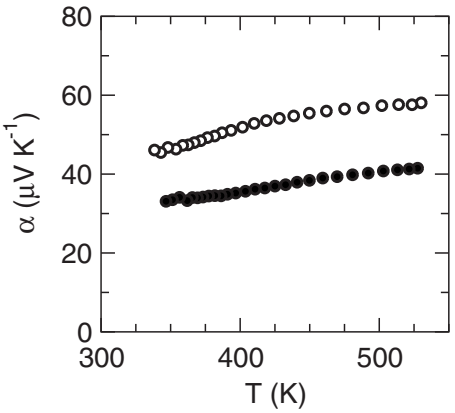

FIG. 4. Seebeck coefficient measurements for the two on-stoichiometry samples measured in Fig. 3.

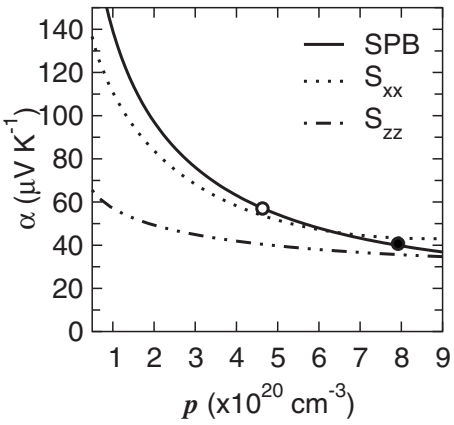

FIG. 5. Seebeck coefficient curves for *p*-type LiZnSb predicted by Madsen at 500 K (S_{xx}, S_{zz}) and from the SPB model of classic Boltzmann transport theory under the CRTA. Experimental 500 K data from the samples reported in this work shown as circles.

~790 K. The trend in resistivity with temperature remains linear until this decomposition temperature. Measurement of the Seebeck coefficient to 750 K reveals no sublimation. The Seebeck coefficient is linear to ~550 K, at which point a weaker temperature dependence is observed, presumably from the loss of degeneracy.

Thermal diffusivity (D) values were determined from laser flash measurements and used to calculate the thermal conductivity ($\kappa = DC_p d$; C_p specific heat; d density). In the absence of specific heat data, the Dulong–Petit value (0.386 J/g K) was employed, yielding the upper curves in Fig. 6. To estimate the lattice thermal conductivity, κ_L, the electronic component of the thermal conductivity is subtracted from κ by employing the Wiedemann–Franz relationship ($\kappa_e = L\sigma T$, where $L = 2.44 \times 10^{-8}$ W Ω K^{-2} is utilized to maintain consistency with Madsen's calculations). The lattice thermal conductivity is found to be between 2 and 3 W/m K at 500 K, and therefore Madsen's assumption of $\kappa_L = 2$ W/m K appears reasonable for LiZnSb near 600 K. The authors note that the Lorenz number is calculated to be between 2.3 and 2.4×10^{-8} W Ω K^{-2} with the CRTA (for all temperatures examined).

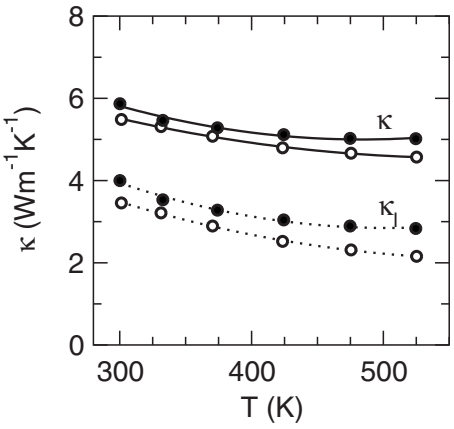

FIG. 6. Thermal conductivity (κ) measurements of two nominally on-stoichiometry LiZnSb samples and the lattice thermal conductivity (κ_l) obtained from subtraction of the electronic thermal conductivity from κ.

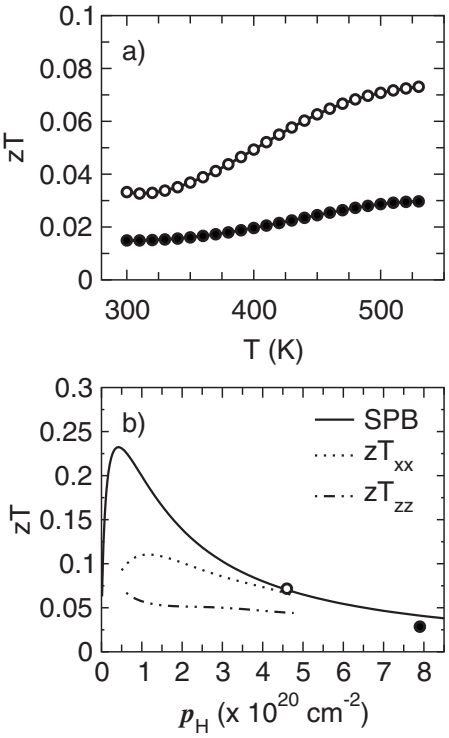

FIG. 7. (a) Figure of merit (zT) of the two p-type LiZnSb samples described in Figs. 3–6. (b) Approximate zT_{xx} *and* zT_{zz} at 500 K with carrier concentration dependence derived from power factor curve by Madsen, a constant $\tau=1\times10^{-14}$ s approximation, and experimentally determined lattice thermal conductivity. Solid curve generated using a SPB model of classic Boltzmann transport theory under the CRTA.

Using polynomial fits to the transport data in Fig. 3–6, the dimensionless figure of merit (zT) is plotted as a function of temperature in Fig. 7(a). Peak zT values of 0.02 and 0.08 are obtained at 525 K for carrier concentrations of 7.9 $\times10^{20}$ and 4.6×10^{20} cm^{-3}, respectively [Fig. 7(b)]. Shown in Fig. 7(b) are three theoretical models for the behavior of zT with carrier concentration (discussed below). The solid line is a classical analysis using Boltzmann transport equations while the two broken curves are obtained from a combination of Madsen's *ab initio* calculations and our experimental results.

To calculate the carrier concentration dependence of zT using Madsen's calculations, estimates of the carrier relaxation time (τ) and lattice thermal conductivity are required ($\kappa_L\sim2.2$ W/m K from our experimental work). After obtaining τ, the τ-dependent power factor and Seebeck curves from Madsen are utilized to calculate the electrical conductivity and the electronic component of the thermal conductivity, and thus zT [broken curves, Fig. 7(b)]. To determine τ, we utilize the Drude model of conductivity ($\tau=\mu m^*/e$) and experimentally determined values for the mobility and effective mass. From these calculations, τ values near 0.7 and 1.2×10^{-14} s are obtained at 500 K for $p_H\sim7$ and 4 $\times10^{20}$ cm^{-3}, respectively; an average value of 1×10^{-14} s is selected for zT estimates. The decrease in τ with increasing carrier density suggests that the CRTA is not rigorously applicable. We note that such a trend is roughly consistent with the theoretical description of carriers scattered by acoustic phonons ($\tau\propto p^{-1/3}$).[13]

The optimized zT for p-type conduction can also be estimated from classical Boltzmann transport theory. The figure of merit can be calculated as a function of the β parameter, which can be determined from an unoptimized sample. In this analysis, the parameter is given by

$$\beta=\frac{\mu_0(m^*/m_e)^{3/2}(T/300)^{5/2}}{\kappa_L},$$

where μ_0 is the carrier mobility in a nondegenerate sample, κ_L is the lattice thermal conductivity obtained utilizing a degeneracy-corrected Lorenz number, L, and m^*/m_e is the effective mass of an electron relative to the rest mass.[12,14] Each of these parameters can be calculated from the experimental data and an assumption regarding the energy dependence of the carrier relaxation time (the CRTA is utilized here). After obtaining β at the desired temperature, zT_{max} can be estimated via the plot of zT_{max} versus β presented by Wood.[14] For this study, we also desire to investigate the difference between the classical and *ab initio* methods, and therefore we will utilize β to calculate zT as a function of carrier concentration [solid curve, Fig. 7(b)].

Here, we assume the relaxation time is independent of energy and calculate the corresponding value of β at 500 K. The equations utilized can be found in a large variety of resources.[12,15] The calculation begins by determining the reduced Fermi energy from the Seebeck coefficient at the desired temperature. The Fermi energy and scattering assumption are then utilized to determine m^*/m_e, μ_0, and L; we note that for the CRTA $\mu_0=\mu$. The calculation yields $\beta(500\ K)=4.8\times10^3$ and 2.5×10^3 $cm^3\ K^{7/2}\ V^{-2}\ C$ for $p_H\sim4$ and $\sim7\times10^{20}$ cm^{-3}, respectively. Utilizing the larger value of $\beta(500\ K)$, the SPB curve in Fig. 7(b) is generated. If the CRTA were not utilized, and carrier mobility is assumed to be dominated by acoustic phonons, then slightly larger $\beta(500\ K)$ and zT_{max} values are obtained due to an increase in μ_0.

The SPB model and the *ab initio* results agree well at high carrier concentrations, while at low carrier concentrations multiband features weaken the Seebeck coefficient in the *ab initio* model, which results in lower zT. Despite not taking multiband features into account, the classical SPB calculation predicts similar thermoelectric performance, and can be obtained by analyzing the transport properties of an unoptimized sample. While SPB analysis suggests that p-type LiZnSb is not well suited for thermoelectric applications; such an investigation offers little insight into the behavior of n-type samples. Therefore, the ability of *ab initio* calculations to evaluate both conduction and valence bands for thermoelectric performance makes first principles computation an invaluable tool in the search for new thermoelectric materials.

In both approaches, we find that p-type LiZnSb is unlikely to be a candidate for thermoelectric applications. However, our analysis indicates that Madsen's prediction for the thermoelectric performance of p-type LiZnSb was fairly accurate. This suggests that n-type LiZnSb may have good thermoelectric performance, as predicted by Madsen. Furthermore, the observation of decomposition at 790 K suggests that operation at 600 K is feasible. However, our ex-

perimental investigation has been limited to *p*-type conduction, and thus we are unable to address the behavior of *n*-type samples.

C. Carrier concentration control

UID LiZnSb is found to be heavily *p*-type. The tendency of Zintl compounds to form *p*-type materials is not limited to LiZnSb. A survey of literature for semiconducting Zintl antimonides finds the room temperature Seebeck coefficients are positive in sign, indicating hole conduction: $Yb_{14}AlSb_{11}$ (+55),[16] $YbZn_2Sb_2$ (+48),[7] $CaZn_2Sb_2$ (+120),[7] $BaZn_2Sb_2$ (+125),[8] $BaGa_2Sb_2$ (+65),[17] $Yb_5In_2Sb_6$ (+30),[18] $Eu_5In_2Sb_6$ (+76),[19] $Ba_4In_8Sb_{16}$ (+70),[20] ErNiSb (+248),[21] and ErPdSb (+233).[21] The semimetals $Yb_{11}Sb_{10}$ (+20) and $Ca_{11}Sb_{10}$ (−5) (Ref. 22) display compensated Seebeck coefficients. In the case of $Yb_{14}AlSb_{11}$, replacing the Al^{3+} with Mn^{2+} or Zn^{2+} has led to extrinsic *p*-type materials, but synthesis of a *n*-type analog has been nontrivial.[23]

Vacancies on either cation site are the most likely source of holes. Every Li vacancy would create a hole ($V_{Li}' + h^{\bullet}$), and Li deficiency could be the result of oxidation during synthesis. Similarly, the high vapor pressure of Zn could contribute to the observed carrier concentration ($V_{Zn}'' + 2h^{\bullet}$). The unequivocal observation of these vacancies in laboratory XRD is challenging due to the low number of vacancies per unit cell required to achieve these doping levels (0.02 carriers per formula unit). No Li_2O was observed in the XRD pattern, but the sensitivity to such a low-*Z* compound is quite weak. Mixed occupancy among the cations may occur (Li and Zn have identical ionic radii), but no carriers are created as long as the total stoichiometry remains constant. Antimony vacancies are unlikely to dominate the UID carrier concentration as deficiencies in Sb occupancy would lead to an electron-rich composition.

To probe the role of cation deficiency in UID LiZnSb, several samples with excess Li and Zn were prepared. Surprisingly, no decrease in hole carrier concentration was observed for any sample and the phase purity and Seebeck coefficient was unaffected by this excess. Also, thus far extrinsic doping has been unsuccessful in forming an *n*-type composition. Given the difficulty in obtaining *n*-type conduction, or even *p*-type samples with $p_H < 10^{20}$ cm^{-3}, we believe the most plausible explanation for the UID carrier density is that the phase width of LiZnSb at the annealing temperature does not include the stoichiometric composition.

IV. CONCLUSION

Experimental characterization of *p*-type LiZnSb followed by classical transport analysis suggests high thermoelectric efficiency is not possible for *p*-type compositions. Good agreement is found between experimental transport values and prior *ab initio* calculations, suggesting the estimates of large *zT* in *n*-type LiZnSb are plausible. Some caution is required, as the valence and conduction bands appear to be quite different. The differences in band structure prevent discussion of the expected *n*-type properties from our experimental *p*-type data.

ACKNOWLEDGMENTS

We thank the DARPA-Nano Materials Program (No. W911NF-08-C-0058) for funding. EST thanks the Beckman Foundation and CJS thanks the Center for Environmental Studies at Harvey Mudd College for support.

[1] G. J. Snyder and E. S. Toberer, Nature Mater. **7**, 105 (2008).
[2] D. J. Singh, Fifth International Conference on Solid-State and Integrated Circuit Technology, 1998 (unpublished), p. 856.
[3] G. K. Madsen, K. Schwarz, P. Blaha, and D. J. Singh, Phys. Rev. B **68**(12), 125212(2003); S. G. Kim, *ibid.* **57**, 6199 (1998).
[4] G. K. H. Madsen, J. Am. Chem. Soc. **128**, 12140 (2006).
[5] T. J. Seebeck, *Magnetische Polarisation der Metalle und Erze durch Temperatur-Differenz* (Wilhelm Engelmann, Leipzig, 1895).
[6] R. R. Heikes and R. W. Ure, *Thermoelectricity: Science and Engineering* (Interscience, New York, 1961); T. Caillat, J. P. Fleurial, and A. Borshchevsky, J. Phys. Chem. Solids **58**, 1119 (1997).
[7] F. Gascoin, S. Ottensmann, D. Stark, S. M. Haile, and G. J. Snyder, Adv. Funct. Mater. **15**, 1860 (2005).
[8] X-J. Wang, M-B. Tang, J-T. Zhao, H-H. Chen, and X-X. Yang, Appl. Phys. Lett. **90**(23), 232107 (2007).
[9] J. G. Snyder, M. Christensen, E. Nishibori, T. Caillat, and B. B. Iversen, Nature Mater. **3**(7), 458 (2004).
[10] J. P. Heremans, V. Jovovic, E. S. Toberer, A. Saramat, K. Kurosaki, A. Charoenphakdee, S. Yamanaka, and G. J. Snyder, Science **321**, 554 (2008).
[11] G. Schroeder and H. U. Schuster, Z. Naturforsch., B Chem. Sci. **30**, 978 (1975).
[12] H. J. Goldsmid, *Applications of Thermoelectricity* (Wiley, London, 1960).
[13] A. H. Wilson, *The Theory of Metals* (Cambridge University Press, Cambridge, England, 1953).
[14] C. Wood, Rep. Prog. Phys. **51**, 459 (1988).
[15] V. I. Fistul, *Heavily Doped Semiconductors* (Plenum, New York, 1969).
[16] E. S. Toberer, C. A. Cox, S. R. Brown, T. Ikeda, A. F. May, S. M. Kauzlarich, and G. J. Snyder, Adv. Funct. Mater. **18**, 2795 (2008).
[17] S. J. Kim and M. G. Kanatzidis, Inorg. Chem. **40**, 3781 (2001).
[18] S.-J. Kim, J. R. Ireland, C. R. Kannewurf, and M. G. Kanatzidis, J. Solid State Chem. **155**, 55 (2000).
[19] S.-M. Park, E. S. Choi, W. Kang, and S-J. Kim, J. Mater. Chem. **12**, 1839 (2002).
[20] S.-J. Kim, S. Hu, C. Uher, and M. G. Kanatzidis, Chem. Mater. **11**, 3154 (1999).
[21] K. Kawano, K. Kurosaki, H. Muta, and S. Yamanaka, J. Appl. Phys. **104**(1), 013714 (2008).
[22] S. R. Brown, S. M. Kauzlarich, F. Gascoin, and G. J. Snyder, J. Solid State Chem. **180**(4), 1414 (2007).
[23] S. R. Brown, S. M. Kauzlarich, F. Gascoin, and G. J. Snyder, Chem. Mater. **18**, 1873 (2006); S. R. Brown, E. S. Toberer, T. Ikeda, C. A. Cox, F. Gascoin, S. M. Kauzlarich, and G. J. Snyder, *ibid.* **20**, 3412 (2008).